Effects of vacancy-solute clusters on diffusivity in metastable Fe-C alloys

Mukul Kabir,[1] Timothy T. Lau,[1,*] Xi Lin,[2] Sidney Yip,[1,3] and Krystyn J. Van Vliet[1,†]

[1]*Department of Materials Science and Engineering, Massachusetts Institute of Technology, Cambridge, Massachusetts 02139, USA*
[2]*Department of Mechanical Engineering and Division of Materials Science and Engineering,*
Boston University, Boston, Massachusetts 02215, USA
[3]*Department of Nuclear Science and Engineering, Massachusetts Institute of Technology, Cambridge, Massachusetts 02139, USA*

Diffusivity in defected crystals depends strongly on the interactions among vacancies and interstitials. Here we present atomistic analyses of point-defect cluster (PDC) concentrations and their kinetic barriers to diffusion in ferritic or body-centered-cubic (bcc) iron supersaturated with carbon. Among all possible point-defect species, only monovacancies, divacancies, and the PDC containing one vacancy and two carbon atoms are found to be statistically abundant. We find that the migration barriers of these vacancy-carbon PDCs are sufficiently high compared to that of monovacancies and divacancies. This leads to decreased self-diffusivity in bcc Fe with increasing carbon content for any given vacancy concentration, which becomes negligible when the local interstitial carbon concentration approaches twice that of free vacancies. These results contrast with trends observed in fcc Fe and provide a plausible explanation for the experimentally observed carbon dependence of volume diffusion-mediated creep in ferritic (bcc) Fe-C alloys. Moreover, this approach represents a general framework to predict self-diffusivity in alloys comprising a spectrum of point-defect clusters based on an energy-landscape survey of local energy minima (formation energies governing concentrations) and saddle points (activation barriers governing mobility).

PACS number(s): 61.72.Lk, 62.20.Hg

I. INTRODUCTION

In crystalline solids, diffusion proceeds as atoms migrate via lattice defects that may be thermally intrinsic or processing induced.[1] There are many diffusion mechanisms, of which vacancy and interstitial diffusion are the most common.[2] In defected crystals and crystalline alloys, prediction of macroscale diffusivity via microscopic mechanisms is further complicated by the potential formation of clusters comprising multiple types and species of point defects (i.e., point-defect clusters, or PDCs). Typically, the concentration of these PDCs is not known or experimentally accessible, even when the overall concentration of atomic species and lattice vacancies is reasonably well quantified. Thus, quantification of how PDCs impact thermally activated processes, such as diffusion-mediated mechanical failure, presents a scientific challenge of technological relevance. Here, we present a computational framework to predict the self-diffusivity in interstitial alloys comprising appreciable PDC populations. We focus our models and simulations on a specific alloy, body-centered-cubic (bcc) iron that approaches supersaturation of both carbon and vacancies.

The strengthening effects of interstitial carbon solute atoms in (i.e., ferritic or bcc) Fe-C alloys are well understood, owing chiefly to the interaction of C with crystalline defects (e.g., dislocations[3] and grain boundaries[3,4]) to resist plastic deformation via dislocation glide. High-strength steels developed for current energy and infrastructure applications include alloys wherein the bcc Fe matrix is thermodynamically supersaturated in carbon. This degree of supersaturation ranges from 0.3 at. % C upon annealing (670 K) (Ref. 4) to 5 at. % C in volumes that include ferritic grain boundaries.[3] It has been demonstrated that the strong affinity of C to Fe vacancies also maintains an order-of-magnitude supersatura-

tion of vacancies via the formation of PDCs comprising multiple C atoms and multiple Fe vacancies.[5,6] This vacancy supersaturation is also stabilized by other solute atoms including hydrogen.[7,8] Self-diffusion in bcc Fe is governed chiefly by vacancy migration, as the alternative self-interstitial migration mechanism is suppressed in (nonirradiated) bcc Fe due to its significantly higher formation energy.[6] Thus, although it is not yet experimentally feasible to determine the spatial or temporal distribution of these PDCs in such defected crystals, it is reasonable to anticipate that processes requiring self-diffusion in the Fe lattice would be affected by the presence and mobility of these PDCs.

Here we report the effect of solute (carbon) concentration on self-diffusion in a dislocation-free volume of single crystal bcc Fe. The formation and binding energies of statistically abundant PDCs are calculated via electronic [first-principles density functional theory (DFT) (Refs. 9 and 10)] and atomistic (many-body semiempirical potential developed previously for this system[11,12]) approaches. Activation barriers of migration are calculated via the nudged elastic band (NEB) method.[13,14] Such calculations are nontrivial, given the many possible and nonredundant configurations and diffusive pathways available to PDCs of increasing size. Self-diffusivity is then calculated for a system comprising statistically abundant PDCs, as a function of temperature and overall alloy composition. We find that in bcc Fe supersaturated with both carbon and vacancies, three PDCs are statistically abundant: monovacancies (Va_1), divacancies (Va_2), and Va_1C_2 clusters. As the migration barrier of the Va_1C_2 cluster significantly exceeds that of the carbon-free PDCs, the self-diffusivity in such defected volumes is controlled by the migration of Va_1 and Va_2. Thus, self-diffusivity decreases with increasing at. % C and becomes negligible when the carbon concentration exceeds twice that of vacancies. The present results are consistent with the experimental observa-

tion that macroscopic creep strain rate decreases with increasing carbon content in bcc Fe-C alloys.[15] Moreover, this framework provides a general approach to relate microscopic point-defect interaction mechanisms to macroscopic properties in crystals of increasingly realistic defect composition, based on an energy-landscape perspective of calculated energy minima and saddle points.

II. METHODOLOGY

Our calculation of migration energies combines three elements of calculation. First, PDC energetics are calculated from DFT and a modified interatomic potential (constructed from such DFT calculations). Second, PDC concentrations are determined from a statistical model, to identify statistically abundant point-defect clusters as a function of overall composition. Third, PDC migration mechanisms and barriers are ascertained from NEB transition state pathway sampling.

Formation energies, binding energies, and migration barriers of PDCs were calculated via both DFT (Refs. 9 and 10) and modified Finnis-Sinclair (MFS) potential.[11] Formation energy of PDCs comprising x Fe vacancies (Va) and y octahedral carbon (C) interstitials is given by[6,16]

$$E^f_{\mathrm{Va}_x\mathrm{C}_y} = E(\mathrm{Va}_x\mathrm{C}_y) - E_0 - xE(\mathrm{Fe}) - yE(\mathrm{C}), \qquad (1)$$

where $E(\mathrm{Va}_x\mathrm{C}_y)$ and E_0 are the free energies of the supercells (neglecting vibrational entropy) with and without the PDC present, respectively. $E(\mathrm{Fe})$ is the reference energy of bulk, defect-free bcc Fe and $E(\mathrm{C})$ is the reference energy of a C atom in vacuum. The corresponding binding energy of the PDC cluster, i.e., the energy gain in forming the PDC from the respective individual point defects is calculated as[16,17]

$$E^b(\mathrm{Va}_x\mathrm{C}_y) = xE^f_{\mathrm{Va}} + yE^f_{\mathrm{C}} - E^f_{\mathrm{Va}_x\mathrm{C}_y}, \qquad (2)$$

where E^f_{C} represents the formation energy of C at the bcc octahedral interstitial site. The spin-polarized DFT calculations were conducted using the VASP code[18,19] with the Perdew-Burke-Ernzerhof exchange-correlation functional[20] and projector augmented wave pseudopotential[21] at a energy cutoff of 400 eV. The calculations were performed with 128-atom supercells and geometry optimization terminated when the force on each atom was <5 meV/Å. Details of the MFS potential are given elsewhere.[11]

Calculation of the PDC spectrum requires a common lattice for the many types of defect clusters, as we have described previously.[6,16] Similarly, for the present case the defect concentration $\mathcal{C}_i$ of a particular PDC ($\mathrm{Va}_x\mathrm{C}_y$) is defined with respect to the bcc Fe lattice

$$\mathcal{C}_i = (\mathcal{C}_\mathrm{v})^x (\mathcal{C}_\mathrm{c})^y \left[\frac{\alpha_i}{\exp\left(\dfrac{-E^b_i}{k_B T}\right) + 1} \right], \qquad (3)$$

where α_i is defined such that $\alpha_i N$ (N being the total number of bcc lattice positions) represents the number of indistinguishable configurations in the lattice for that particular defect cluster species.[16]

We constrained the total carbon $\mathcal{C}^\mathrm{total}_\mathrm{c}$ and vacancy concentration $\mathcal{C}^\mathrm{total}_\mathrm{v}$ to be equal to the sum over all PDC species,

$$\mathcal{C}^\mathrm{total}_\mathrm{c} = \sum_\mathrm{clusters} y\mathcal{C}_{\mathrm{Va}_x\mathrm{C}_y},$$

$$\mathcal{C}^\mathrm{total}_\mathrm{v} = \sum_\mathrm{clusters} x\mathcal{C}_{\mathrm{Va}_x\mathrm{C}_y}. \qquad (4)$$

This approach enables calculation of PDC concentrations for any arbitrary, total concentration of carbon and vacancies.

Under the transition state approximation, the diffusion rate of a defect species in solids can be written as

$$\Gamma = \tilde{\nu} e^{-(E_m/k_B T)}, \qquad (5)$$

where E_m is the migration barrier of the process (i.e., the energy required to carry the defect from an initial equilibrium position to a saddle point) and $\tilde{\nu}$ is the frequency prefactor. For temperatures far below the melting temperature, the atomic positions in crystalline solids do not deviate greatly from their equilibrium positions. Hence it is reasonable to invoke the harmonic approximation of the transition state theory to calculate the frequency prefactor $\tilde{\nu}$, and is given by[22,23]

$$\tilde{\nu} = \frac{\displaystyle\prod_i^{3N} \nu_i^\mathrm{initial}}{\displaystyle\prod_i^{3N-1} \nu_i^\mathrm{saddle}}, \qquad (6)$$

where ν_i are the normal vibration modes (phonons). Note that the product in the denominator excludes the imaginary frequency corresponding to the unstable mode for the transition state. We determined the minimum-energy path for each migration and the corresponding migration energy barrier E_m using climbing-image nudged elastic band method.[13,14] In NEB, a set of intermediate states (images) are distributed along the reaction path connecting known initial and final states. To ensure the continuity of the reaction path, the images are coupled with elastic forces and each intermediate state is fully relaxed in the hyperspace perpendicular to the reaction coordinate.

III. RESULTS AND DISCUSSION

To predict the effect of C concentration on Fe self-diffusivity for Fe-C alloys comprising a diverse PDC population, it is necessary to first predict the concentration of PDCs, and next determine the migration barriers for the statistically abundant PDCs. Here we detail the results of these calculations, which naturally require evaluation of multiple migration pathways.

A. Point-defect clusters: Formation and abundance

It has been established, both experimentally[24] and theoretically,[6,11,17,25] that solute atoms of intermediate size (e.g., N, C, and O) in a bcc lattice are more stable at the octahedral sites. This introduces a tetragonal distortion to the neighboring Fe lattice.[26] The relaxation of the nearest Fe atoms can be calculated as $\frac{\Delta d_i}{d_i^0}$, where d_i^0 is the ith nearest-

TABLE I. Calculated binding energies (E^b) using DFT and MFS potential are in good agreement. The crystallographic directions $\langle ijk \rangle$ refer to the orientation of the Fe double vacancies. Binding energies for the clusters containing more than two carbon atoms per Fe vacancy are not shown here (see Ref. [6]).

Defect cluster	E^b (eV)	
	DFT	MFS
Va_1C_1	0.53	0.76
Va_1C_2	1.46	1.73
$Va_2\langle 100 \rangle$	0.18	0.21
$Va_2C_1\langle 100 \rangle$	1.05	1.05
$Va_2C_2\langle 100 \rangle$	1.84	1.65
$Va_2C_3\langle 100 \rangle$	2.31	2.25
$Va_2C_4\langle 100 \rangle$	3.20	3.13
$Va_2\langle 111 \rangle$	0.12	0.14
$Va_2C_1\langle 111 \rangle$	0.80	0.93
$Va_2C_2\langle 111 \rangle$	1.93	1.61
$Va_2C_3\langle 111 \rangle$	2.57	2.39
$Va_2C_4\langle 111 \rangle$	3.62	3.09

neighbor (NN) solute-Fe distance before relaxation and $\Delta d_i (= d_i - d_i^0)$ is the change in distance due to relaxation. The calculated relaxations due to octahedral C in bcc Fe $\left[\frac{\Delta d_1}{d_1^0} = 25\% \right.$ (DFT) and 22% (MFS) and $\frac{\Delta d_2}{d_2^0} = -1.5\%$ (DFT) and -1.6% (MFS)$\left.\right]$ are in good agreement with x-ray diffraction measurement[26] and previous theoretical calculation.[17] In contrast, while forming Va_1C_1 complex in the presence of Fe vacancy, the carbon atom relaxes from the octahedral position toward the vacancy and the calculated vacancy-carbon distances are $0.41a_0$ (DFT) and $0.36a_0$ (MFS), which are consistent with positron annihilation experiments.[27]

Calculated binding energies E^b for the PDCs are given in Table I. The results using our previously developed MFS potential[11] are in good agreement with DFT results, as expected from the DFT-based construction this MFS potential.[11] The binding energy for the Va_1C_1 complex, $E^b(Va_1C_1)$, is in good agreement with previous theoretical results.[17,28–30] In contrast, current experimental results range appreciably, $0.4 \leq E^b(Va_1C_1) \leq 1.1$ eV, varying with experimental technique and sample preparation details.[31–34] The magnitude of $E^b(Va_1C_1)$ predicted from resistivity measurements on low-temperature irradiated pure and carbon-doped bcc Fe is comparatively high (1.1 eV).[34] Magnetic-aftereffect measurement predicts a range of $0.1 \leq E^b(Va_1C_1) \leq 0.65$ eV,[32] whereas positron annihilation data suggests an upper limit of 0.75 eV.[33] Calculated binding energy for the vacancy-carbon complex containing two carbon atoms, Va_1C_2, is in good agreement with previous DFT calculation.[17] In agreement with previous experimental findings,[34,35] it should be noted from Table I that it is energetically favorable to add a carbon atom to a pre-existing Va_1C_1 complex than to form a new Va_1C_1 complex.

It is observed experimentally that solute atoms in bcc Fe serve to increase the vacancy concentration well above the
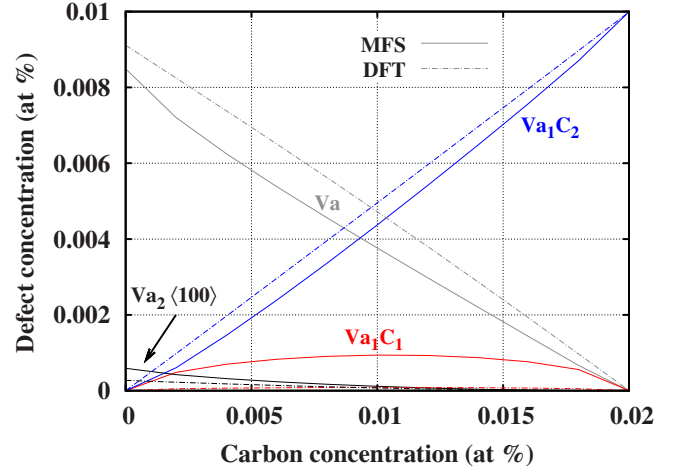

FIG. 1. (Color online) Abundance of PDCs as a function of carbon content for an assumed vacancy concentration (10^{-4}) at 160 °C (433 K). Concentrations of Va_1 and $Va_2\langle 100 \rangle$ decrease with increasing C, which is accompanied by an increase in Va_1C_2 cluster concentration. Concentration of other PDCs are orders of magnitude lower than these abundant PDCs.

thermodynamically predicted levels in an otherwise perfect lattice.[5,7,8] Our previous DFT calculations showed that this is indeed the case for carbon-rich ferrite and found that Va_1C_2 complexes are the most abundant vacancy-containing defect cluster.[6] In general, we find that for any assumed vacancy concentration, the free monovacancy and divacancy concentrations decrease with increase in available carbon content in the solid solution (Fig. 1). Consequently, Va_1C_2 concentration increases due to comparatively high thermodynamic stability. The relative abundance of Va_1C_1, Va_2C_1, and Va_2C_2 clusters and all other larger vacancy-carbon PDCs containing more than two C atoms are found to be negligible.[6] Although Fig. 1 shows this trend for an assumed constant vacancy concentration of 10^{-4} and at a specific temperature of 433 K (an annealing temperature for high carbon steel considered in our previous studies[6,11]), this behavior is found to be generic for any vacancy concentration and temperatures below the Curie temperature at which bcc Fe transforms to fcc Fe.

B. Single-defect migration

Having determined the statistical abundance, we next calculate the migration barriers for PDCs corresponding to various possible migration pathways. Isolated point defects, Va_1 and C_1, are the smallest point defects, and thus the migration mechanisms are simpler compared to the large PDCs. Migration of a single vacancy in a bcc lattice has only two possible migration pathways: along the $\langle 100 \rangle$ and $\langle 111 \rangle$ (Fig. 2) directions. Migration along the $\langle 100 \rangle$ directions requires much higher energy of ~ 3.5 eV. In comparison, diffusion along the $\langle 111 \rangle$ direction requires minimum energy, and is thus the minimum-energy pathway for vacancy diffusion. The calculated MFS-NEB migration barrier (0.84 eV) agrees well with the present first-principles DFT-NEB calculation (0.75 eV) and also with previous DFT calculations with different level of approximations (within ~ 0.1 eV).[36,37] However, the ex-
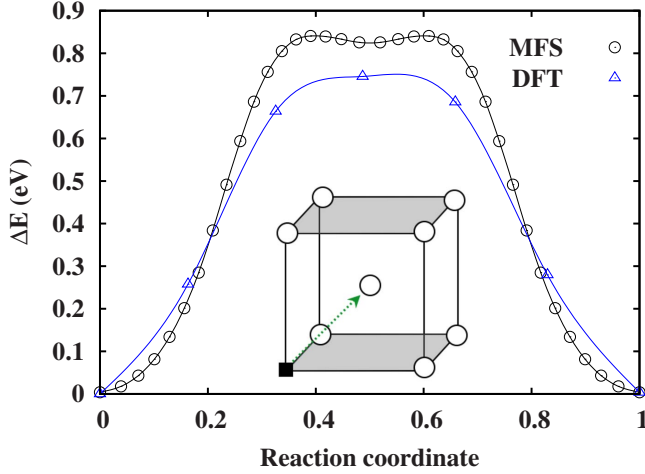
FIG. 2. (Color online) Monovacancy migration along $\langle 111 \rangle$ directions. The DFT and MFS results are in good agreement. Diffusion along $\langle 100 \rangle$ directions require much higher energy (~ 3.5 eV) and is not shown. Filled square represents the Fe vacancy.

TABLE II. Migration energy barrier for Va_1 diffusion in Va_1C_1 cluster. $i \rightarrow j$ ($j \rightarrow i$) represents forward (backward) vacancy jump, as represented in Fig. 3(a). Present MFS-NEB results are compared with Ref. 47.

| | Migration energy (eV) | | | |
| | $i \rightarrow j$ | | $j \rightarrow i$ | |
Vacancy jump	Present	Ref. 47	Present	Ref. 47
$1 \rightarrow 2$	0.59	0.49	0.18	0.28
$1 \rightarrow 9$	1.84	1.60	0.87	0.64
$2 \rightarrow 3$	0.98	0.79	0.83	0.61
$2 \rightarrow 4$	0.81	0.63	0.60	0.47
$2 \rightarrow 5$	1.30	0.95	0.96	0.73
$2 \rightarrow 6$	0.81	0.63	0.60	0.47
$2 \rightarrow 7$	0.86	0.63	0.67	0.50
$2 \rightarrow 8$	0.86	0.68	0.65	0.48

perimental $\langle 111 \rangle$-migration barrier is widely scattered (0.55–1.28 eV) (Refs. 5, 38, and 39) and remains disputed despite numerous experimental attempts over decades.[5,38–43] This wide experimental range is attributed to difficulties in preparing high purity bcc Fe, the high sensitivity of Fe vacancies to interstitial solutes, and also in the interpretation of experimental data.[5,27,38–43]

In contrast, the (octahedral) C solute atom has only a single expected migration pathway defined by the octahedral interstitial lattice. For such migration, it is intuitive to assume that the tetrahedral site connecting two neighboring octahedral sites would be the transition state (saddle point). The energy difference between the tetrahedral and octahedral state might be a good estimate of the activation energy for such migration.[17,25] However, without this *a priori* assumption, we carried out NEB calculations for C migration in vacancy-free bcc Fe. We indeed find the tetrahedral carbon state as the saddle point. The calculated MFS migration energy is smaller (0.64 eV) than that predicted by DFT (0.86 eV), which is in good agreement with experimentally measured barriers ranging 0.81–0.88 eV.[27,34,44,45]

The solute (carbon) diffusion coefficient is a function of jump rate Γ, $D_c = \frac{1}{6} a_c^2 \Gamma$. Neglecting the formation entropy,

ΔS_f, the diffusion coefficient becomes, $D_c = D_0 \exp$ ($-E_m^c / k_B T$) with $D_0 = \frac{1}{6} a_c^2 \tilde{\nu}$. Here a_c is the jump distance (between two nearest-neighbor octahedral sites in case of C diffusion) and E_m^c is the corresponding C migration barrier. Within the Einstein approximation, we considered the vibrational modes of the atoms near the defect, which significantly reduced the size of the Hessian matrix to calculate phonon frequencies. The calculated prefactor $D_o(C) = 3.48 \times 10^{-7}$ m^2/s (DFT) and 4.72×10^{-7} m^2/s (MFS) are in good agreement with previous theoretical predictions[17,25] and the average experimental $D_o(C)$ below 350 K, 1.67×10^{-7} m^2/s.[46]

C. Point-defect cluster migration

The number of possible migration mechanisms increases rapidly with defect cluster size and thus becomes increasingly expensive computationally for DFT-NEB approach. Instead we have used NEB-MFS to survey minimum-energy pathways for larger clusters. Although the Va_1C_1 cluster abundance in the bcc Fe-C alloy is negligible, we studied dissociative and associative migration pathways for this complex to compare with recent results.[47] Schematic positions of vacancy and carbon for dissociative and full (asso-
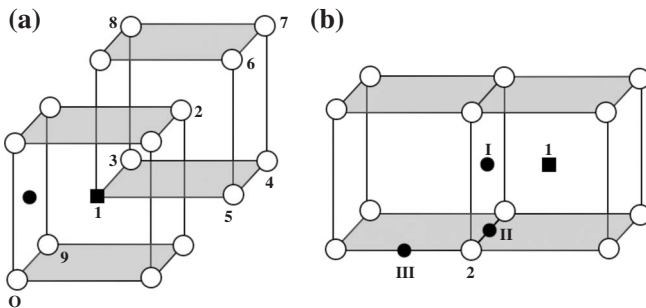

FIG. 3. (Color online) Migration of the Va_1C_1 complex. Schematic representation of (a) dissociative and (b) associative migrations. Point defects are indicated by Arabic (Fe vacancy) and Roman (carbon) numerals. Position O(0,0,0) in (a) represents the origin. Similar conventions have been used throughout. (c) and (d) Migration pathways corresponding to the mechanisms described in (a) and (b), respectively.
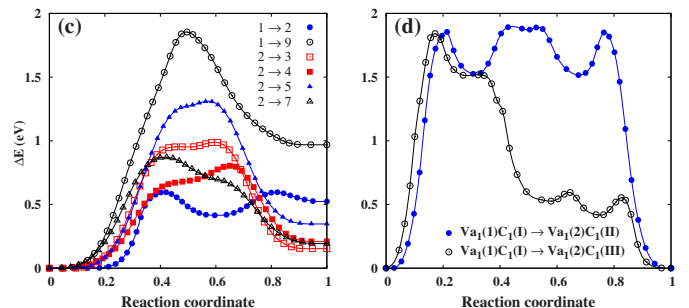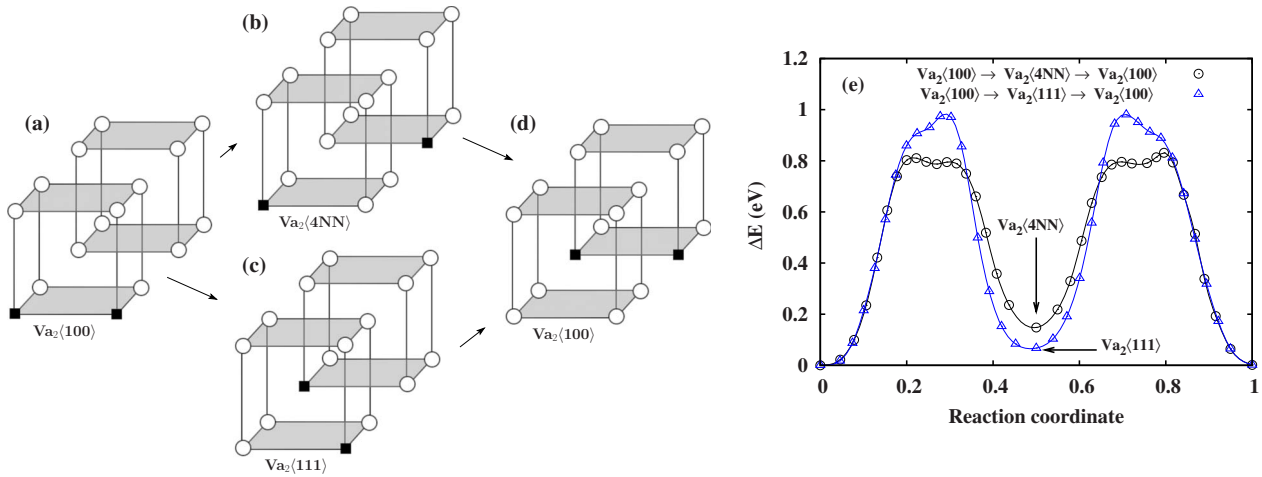
FIG. 4. (Color online) Migration of the $Va_2\langle100\rangle$ cluster. (a) Migration mechanisms via dissociative $Va_2\langle4NN\rangle$ and associative $Va_2\langle111\rangle$ intermediates. (b) Minimum-energy pathways for the mechanisms described in (a).

ciative) migration of Va_1C_1 cluster is shown in Figs. 3(a) and 3(b). The minimum-energy paths are shown in Figs. 3(c) and 3(d) and the migration barriers are tabulated in Table II. Present values for the migration barriers are systematically larger by 0.15–0.20 eV compared to the theoretical study of Tapasa *et al.*[47] This can be attributed to different computational techniques in obtaining the migration barriers as well as to the use of different potentials to represent Fe-C interactions. The potential used in the present study was specifically developed to accurately predict both the configurations and energetics of carbon-rich clusters.[11] In contrast to the dissociative migrations, the associative Va_1C_1 migration requires significantly higher energy [Figs. 3(b) and 3(d)]. It is important to notice here that for all dissociative Va migration pathways [Fig. 3(c) and Table II], the energetic cost for a vacancy to jump toward carbon is much lower than the Va jump away from carbon, i.e., a vacancy is more likely to rebind to the carbon than to dissociate from carbon.

There exist two distinct divacancy configurations, $Va_2\langle111\rangle$ and $Va_2\langle100\rangle$. Formation of $Va_2\langle100\rangle$ is favorable compared to $Va_2\langle111\rangle$ (Table I) and thus the divacancy cluster in $\langle100\rangle$ configuration is more statistically abundant. The divacancy in either of these configurations migrates by successive monovacancy jumps. Figure 4(a) illustrates that the $Va_2\langle100\rangle$ cluster can migrate along $\langle111\rangle$ directions by two distinct mechanisms: (i) through a dissociative $Va_2\langle4NN\rangle$ intermediate [two vacancies separated by four nearest neighbors shown in Fig. 4(b)] with a migration barrier of E_m =0.80 eV, which is slightly lower than that of monovacancy migration; (ii) through a $Va_2\langle111\rangle$ intermediate [Fig. 4(c)]. The migration barrier for the second mechanism is almost 0.2 eV higher [Fig. 4(e)]. In comparison, DFT-calculated activation barriers corresponding to these two migration mechanisms are 0.74 eV and 0.85 eV, respectively. The migration barrier of the former mechanism agrees within 0.12 eV with the equivalent mechanism calculated via a different implementation of DFT and transition state sampling.[37] An energetically equivalent barrier of 0.97 eV can also be realized by a slight variant of the second mechanism, where the final orientation of the $Va_2\langle100\rangle$ cluster is rotated by 90°.

In contrast, migration of the $Va_2\langle111\rangle$ cluster is more energetically expensive by ~0.15 eV. We have detailed the migration mechanisms and corresponding activation barriers of the $Va_2\langle111\rangle$ in Appendix. Due to the lower concentration and higher barriers of $Va_2\langle111\rangle$ migration, the concentration and migration barriers corresponding to $Va_2\langle100\rangle$ were thus considered to represent the contribution of divacancy mobility in our subsequent calculation of Fe self-diffusivity as a function of C concentration.

The most prevalent Va-C complex at high carbon concentrations of interest is found to be the Va_1C_2 cluster (Fig. 1). Figures 5(a) and 5(b) summarizes different migration mechanisms and corresponding migration barriers of this complex. This PDC can migrate through dissociation into smaller PDCs ($Va_1C_2 \rightarrow Va+2C$ indicating dissociation into three isolated point defects and $Va_1C_2 \rightarrow Va_1C_1+C$ indicating dissociation into a smaller Va-C PDC and isolated carbon). These migrations are equally probable (E_m=2.28 eV and 2.22 eV barriers, respectively). Further, these barriers are considerably higher than monovacancy and divacancy migrations, and thus these carbon-containing PDCs will not migrate and contribute appreciably to the self-diffusivity. Similar to the Va_1C_1 complex, the Va migration barriers toward
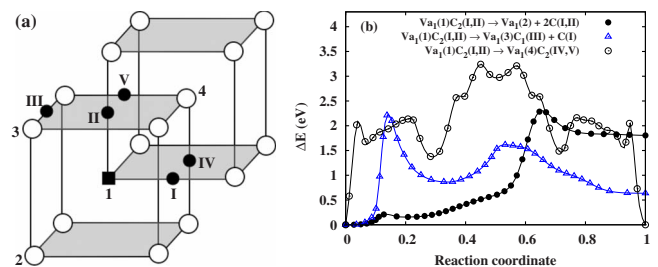

FIG. 5. (Color online) Migration of statistically abundant vacancy-carbon complex, Va_1C_2 via dissociation into either three isolated point defects (●), Va_1C_1 cluster and isolated C (△), or a fully reconstituted Va_1C_2 PDC (○). (a) The initial and final positions of point defects for these mechanisms are indicated by parenthetical Arabic numerals (Va) and Roman numerals (c). (b) Migration barriers for different mechanisms.

the carbon atoms for these dissociative Va_1C_2 migrations are much smaller (0.48 eV and 1.58 eV, respectively) than the corresponding Va migration away from the carbon atoms [Fig. 5(b)], i.e., the reformation of the Va_1C_2 complex is more likely than the dissociation of this PDC. Although both the carbon and vacancy move together during the dissociative $Va_1C_2 \rightarrow Va_1C_1 + C$ migration, the analysis of the trajectories of both the Va and C [Δ in Fig. 5(b)] enables us to correlate the energetic peak (at reaction coordinate ~0.15) with dominant motion of the C, and the shoulder (at reaction coordinate ~0.55) with dominant motion of the Va. Compared to these dissociative migration mechanisms, migration of this PDC to maintain an intact Va_1C_2 cluster is less probable due to a much higher energy barrier [3.24 eV, Fig. 5(b)].

D. Self-diffusivity and carbon concentration

We found that monovacancies and divacancies are the only point-defect species with comparable migration energies. In contrast, the prevalent Va_1C_2 cluster is essentially immobile. Therefore, the diffusivity in ferritic or bcc Fe-C alloys is dominated by monovacancies and divacancies, and the Fe self-diffusivity can be written as a sum of these independent contributions,[48,49]

$$D^* = a_v^2 \mathcal{C}_v \nu_v e^{-(E_m^v/k_BT)} f_v + 2a_{2v}^2 \mathcal{C}_{2v\langle 100 \rangle}$$
$$\times [\nu_I e^{-(E_m^I/k_BT)} + \nu_{II} e^{-(E_m^{II}/k_BT)}] f_{2v}. \qquad (7)$$

Here a is the jump distance calculated from the atomic configurations, $\mathcal{C}$ are the PDC species concentrations, $\tilde{\nu}$ is the jump frequency [calculated from Eq. (6)], f is the jump correlation factor, and E_m are the migration barriers. The frequencies and energy barriers for $Va_2\langle 100 \rangle \rightarrow Va_2\langle 4NN \rangle \rightarrow Va_2\langle 100 \rangle$ and $Va_2\langle 100 \rangle \rightarrow Va_2\langle 111 \rangle \rightarrow Va_2\langle 100 \rangle$ migrations (Fig. 4) are labeled with I and II, respectively. The correlation factor for divacancies, f_{2v}, depends on the ratio of the jump frequencies, $\tilde{\nu}_I / \tilde{\nu}_{II}$, corresponding to these mechanisms,[48,49] for which we used the functional form introduced by Belova *et al.*[50] through Monte Carlo simulations. We find that self-diffusivity decreases rapidly with increasing carbon content in the matrix (Fig. 6) and further that this general conclusion is independent of temperature (below 1180 K at which bcc Fe is the stable crystal structure). The reason for such decrease in D^* with increasing carbon concentration is straightforward in terms of relative mobility of the PDC spectrum. First, the concentrations of mobile Va_1 and Va_2 decrease with increasing carbon content. Second, with increasing carbon content, the concentration of Va_1C_2 PDCs also increases. These PDCs are effectively immobile due to their high migration barrier determined above. Given our finding that diffusivity is dominated by monovacancies and divacancies, we proceed with the hypothesis that diffusivity vanishes with decreasing vacancy concentration [see Eq. (7)]. Thus, as Fig. 6 shows, D^* vanishes when there are no longer free (monovacancies or divacancies) vacancies present. This vanishing free vacancy population and diffusivity naturally occurs when the carbon concentration is twice the vacancy concentration, at which point all free vacancies are subsumed into Va_1C_2 clusters.
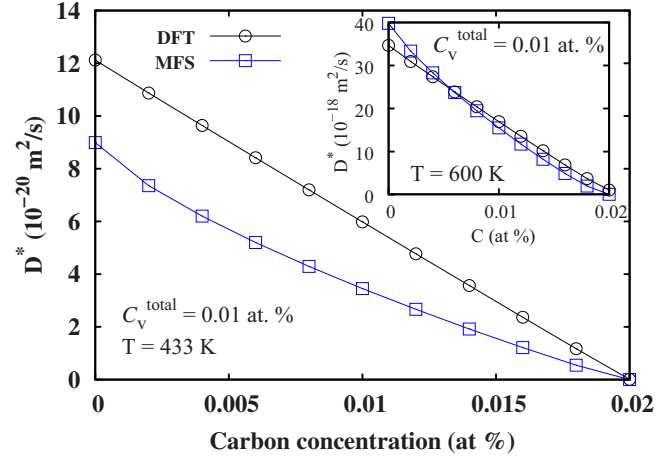

FIG. 6. (Color online) Fe self-diffusion decreases with increase in carbon content in bcc Fe matrix. Modified Finnis-Sinclair potential calculations are in good agreement with the first-principles DFT calculations. Diffusivity becomes negligible when the carbon concentration in the matrix becomes twice that of the Fe vacancies.

Note that the present calculations consider the concentration of carbon in the bcc Fe matrix or lattice, and thus lattice diffusion. Clearly, the *total* carbon concentration in such alloys also includes finite carbon concentration at dislocations, grain boundaries, and other phases.[51] However, the overall trend of D^* with carbon concentration in the *lattice* is preserved in such cases of additional complexities. The present result for bcc Fe, wherein self-diffusivity decreases with increasing carbon content (Fig. 6) contrasts with the experimentally observed carbon dependence in the other high-temperature polymorph, (austenetic) fcc Fe-C. Carbon enhances self-diffusivity by nearly one order of magnitude upon addition of 1 wt % C in the fcc Fe matrix.[52,53] This enhancement is due to the fact that in fcc Fe, the smallest vacancy-carbon complex, namely, the Va_1C_1 cluster, contributes considerably to self-diffusion. In contrast, for bcc Fe we find this complex is not statistically abundant in the PDC spectrum, and thus does not contribute to self-diffusion. Similar carbon concentration dependent decreases in self-diffusion for bcc Fe have been reported by Fu *et al.*[54] However, that previous theoretical approach relied on an important *a priori* assumption that all PDCs containing C are immobile, assumed the atomic jump frequency, and neglected the contribution of divacancy clusters to self-diffusion. There is no explicit experimental measurement of Fe self-diffusivity as a function of carbon content in bcc Fe, our results on dislocation-free single-crystal bcc Fe are consistent with the experimental observations of macroscopic creep strain rates (at a given applied stress and temperature in the power-law creep regime) decreasing with increasing total carbon content in polycrystalline Fe-C alloys.[15] This observed creep operates by a dislocation climb mechanism (in accordance from its power-law stress dependence) and, as a result, is related to diffusivity of lattice vacancies.[55–57] (Although the quantitative measurement of the differential distribution of carbon in different regions of single-crystalline and polycrystalline alloys is a current experimental challenge, it is quite plausible that the carbon concentration
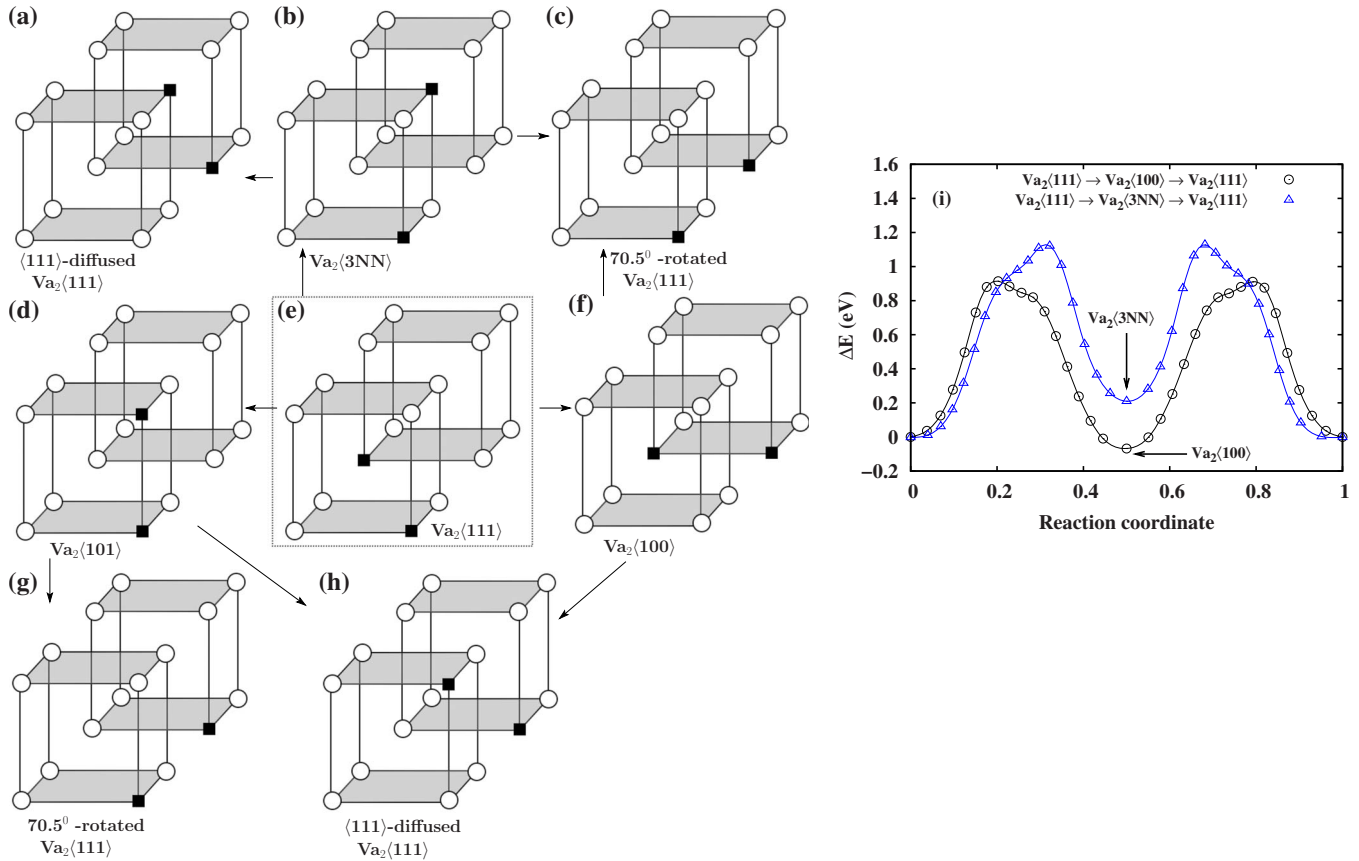
FIG. 7. (Color online) Migration of the $Va_2\langle 111\rangle$ cluster. (a)–(h) Different migration mechanisms through various intermediates. (i) Minimum-energy pathways of $Va_2\langle 111\rangle$ migration to a final 70.5°-rotated $Va_2\langle 111\rangle$ cluster through the dissociative $Va_2\langle 3NN\rangle$ and associative $Va_2\langle 100\rangle$ intermediates.

within the bcc Fe matrix increases with increasing total carbon content in bcc Fe-C alloy.) The present methodology and results thus present a quantitative dependence of self-diffusion on interstitial solute in (single-crystalline) structural alloys, and is also consistent with the qualitative solute dependence of steady-state creep in polycrystalline alloys.[15]

IV. SUMMARY

Here, we employed atomistic simulations combined with statistical theory to study the abundance and microscopic migration mechanism of various point-defect clusters in ferritic (bcc) Fe-C alloys. For this system of interest, we find that self-diffusivity within dislocation-free regions of the matrix decreases with increasing carbon content and becomes negligible as carbon concentration in the lattice approaches twice that of the vacancy concentration. We suggest that the experimental trend in such alloys, decreasing creep rate with increasing carbon content, can be attributed in part to the reduced number of mobile vacancies in the matrix with increasing carbon content. More generally, this modeling and simulation approach demonstrates the potential to rapidly survey the energetic minima (which govern PDC concentrations) and saddle points (which govern PDC mobility) of complex structural alloys for plausible, kinetically controlled diffusion, and deformation mechanisms.

APPENDIX: MIGRATION MECHANISM OF $Va_2\langle 111\rangle$ CLUSTER

Although the divacancy cluster in the $\langle 111\rangle$ configuration is not statistically abundant in the PDC spectrum, we calculated the corresponding migration barriers to compare with the $\langle 100\rangle$ counterpart. Indeed, the activation barrier for the most probable migration of divacancy in this configuration is ~ 0.15 eV higher than in $\langle 100\rangle$ configuration. Different possible migration paths for $Va_2\langle 111\rangle$ are shown in Figs. 7(a)–7(h). A $Va_2\langle 111\rangle$ cluster [Fig. 7(e)] can migrate to a 70.5°-rotated $Va_2\langle 111\rangle$ configuration [Figs. 7(c) and 7(g)] in two possible paths via different intermediate states of varying NN distances. The energy cost for the migration through a $Va_2\langle 3NN\rangle$ intermediate [Fig. 7(b)] is ~ 0.20 eV higher compared to the migration via $Va_2\langle 100\rangle$ configuration [Fig. 7(f)]. Corresponding migration barriers are shown in Fig. 7(i). A $Va_2\langle 111\rangle$ cluster [Fig. 7(e)] can also completely

diffuse to $\langle 111 \rangle$ direction [Figs. 7(a) and 7(h)] through one of these (Va$_2\langle$3NN$\rangle$ or Va$_2\langle$100$\rangle$) intermediates. We see the migration barriers depend only on the intermediates (dissoci-ated $\langle$3NN$\rangle$ or bound $\langle$100$\rangle$ cluster) and are independent of the final divacancy configurations, i.e., whether it is rotated by 70.5° or diffuses only along $\langle 111 \rangle$ direction.

*Present address: Stanford Law School, Stanford, California 94305, USA.

†Corresponding author.

[1] P. Shewmon, *Diffusion in Solids* (Minerals, Metals and Materials Society, Warrendale, 1989).

[2] N. Peterson, in *Solid State Physics*, edited by F. Seitz, D. Turnbull, and H. Ehrenreich (Academic Press, New York, 1968), Vol. 22.

[3] J. Wilde, A. Cerezo, and G. D. W. Smith, Scr. Mater. **43**, 39 (2000).

[4] S. Ohsaki, K. Hono, H. Hidaka, and S. Takaki, Scr. Mater. **52**, 271 (2005).

[5] A. Vehanen, P. Hautojärvi, J. Johansson, J. Yli-Kauppila, and P. Moser, Phys. Rev. B **25**, 762 (1982).

[6] C. J. Först, J. Slycke, K. J. Van Vliet, and S. Yip, Phys. Rev. Lett. **96**, 175501 (2006).

[7] R. B. McLellan and Z. R. Xu, Scr. Mater. **36**, 1201 (1997).

[8] V. G. Gavriljuk, V. N. Bugaev, Y. N. Petrov, A. Tarasenko, and B. Z. Yanchitski, Scr. Mater. **34**, 903 (1996).

[9] P. Hohenberg and W. Kohn, Phys. Rev. **136**, B864 (1964).

[10] W. Kohn and L. J. Sham, Phys. Rev. **140**, A1133 (1965).

[11] T. T. Lau, C. J. Först, X. Lin, J. D. Gale, S. Yip, and K. J. Van Vliet, Phys. Rev. Lett. **98**, 215501 (2007).

[12] T. T. Lau, X. Lin, S. Yip, and K. J. Van Vliet, Scr. Mater. **60**, 399 (2009).

[13] G. Henkelman, B. P. Uberuaga, and H. Jónsson, J. Chem. Phys. **113**, 9901 (2000).

[14] G. Henkelman and H. Jónsson, J. Chem. Phys. **113**, 9978 (2000).

[15] C. K. Syn, D. R. Lesure, O. D. Sherby, and E. M. Taleff, Mater. Sci. Forum **426-432**, 853 (2003).

[16] P. R. Monasterio, T. T. Lau, S. Yip, and K. J. Van Vliet, Phys. Rev. Lett. **103**, 085501 (2009).

[17] C. Domain, C. S. Becquart, and J. Foct, Phys. Rev. B **69**, 144112 (2004).

[18] G. Kresse and J. Hafner, Phys. Rev. B **47**, 558 (1993).

[19] G. Kresse and J. Furthmüller, Phys. Rev. B **54**, 11169 (1996).

[20] J. P. Perdew, K. Burke, and M. Ernzerhof, Phys. Rev. Lett. **77**, 3865 (1996).

[21] P. E. Blöchl, Phys. Rev. B **50**, 17953 (1994).

[22] G. H. Vineyard, J. Phys. Chem. Solids **3**, 121 (1957).

[23] G. H. Vineyard and G. J. Dienes, Phys. Rev. **93**, 265 (1954).

[24] G. K. Williamson and R. E. Smallman, Acta Crystallogr. **6**, 361 (1953).

[25] D. E. Jiang and E. A. Carter, Phys. Rev. B **67**, 214103 (2003).

[26] A. W. Cochardt, G. Schoek, and H. Wiedersich, Acta Metall. **3**, 533 (1955).

[27] P. Hautojärvi, J. Johansson, A. Vehanen, J. Yli-Kauppila, and P. Moser, Phys. Rev. Lett. **44**, 1326 (1980).

[28] R. A. Johnson, G. J. Dienes, and A. C. Damask, Acta Metall. **12**, 1215 (1964).

[29] V. Rosato, Acta Metall. **37**, 2759 (1989).

[30] S. Simonetti, M. E. Pronsato, G. Brizuela, and A. Juan, Phys.

Status Solidi B **244**, 610 (2007).

[31] R. A. Arndt and A. C. Damask, Acta Metall. **12**, 341 (1964).

[32] F. Walz and H. J. Blythe, Phys. Status Solidi A **104**, 343 (1987).

[33] R. B. McLellan and M. L. Wasz, Phys. Status Solidi A **110**, 421 (1988).

[34] S. Takaki, J. Fuss, H. Kuglers, U. Dedek, and H. Schultz, Radiat. Eff. Defects Solids **79**, 87 (1983).

[35] M. Weller, J. Phys. (France) **46**, C10 (1985).

[36] C. Domain and C. S. Becquart, Phys. Rev. B **65**, 024103 (2001).

[37] C.-C. Fu, J. Torre, F. Willaime, J.-L. Bocquet, and A. Barbu, Nature Mater. **4**, 68 (2005).

[38] H.-E. Schaefer, K. Maier, M. Weller, D. Herlach, A. Seeger, and J. Diehl, Scr. Metall. **11**, 803 (1977).

[39] A. Seeger, Phys. Status Solidi A **167**, 289 (1998).

[40] M. Kiritani, H. Takata, K. Moriyama, and F. Fujita, Philos. Mag. A **40**, 779 (1979).

[41] F. Walz, H. J. Blythe, and H. Kronmüller, Phys. Status Solidi A **61**, 607 (1980).

[42] S. Takaki and H. Kimura, Scr. Metall. **10**, 1095 (1976).

[43] J. Diehl, U. Merbold, and M. Weller, Scr. Metall. **11**, 811 (1977).

[44] A. D. Le Claire, in *Numerical Data and Functional Relationships in Science and Technology*, edited by H. Mehrer, Landolt-Börnstein, New Series, Group III, Vol. 26 (Springer-Verlag, Berlin, 1990).

[45] C. A. Wert, Phys. Rev. **79**, 601 (1950).

[46] J. R. G. da Silva and R. B. McLellan, Mater. Sci. Eng. **26**, 83 (1976).

[47] K. Tapasa, A. Barashev, D. Bacon, and Y. Osetsky, Acta Mater. **55**, 1 (2007).

[48] H. Mehrer, J. Phys. F: Met. Phys. **3**, 543 (1973).

[49] H. Mehrer, J. Nucl. Mater. **69-70**, 38 (1978).

[50] I. V. Belova, D. S. Gentle, and G. E. Murch, Philos. Mag. Lett. **82**, 37 (2002).

[51] Y. Shima, Y. Ishikawa, Y. Y. H. Nitta, K. Mimura, M. Isshiki, and Y. Iijima, Mater. Trans. **43**, 173 (2002).

[52] J. A. Slane, C. Wolverton, and R. Gibala, Metall. Mater. Trans. A **35**, 2239 (2004).

[53] D. R. Lesuer, C. K. Syn, J. D. Whittenberger, M. Carsi, O. A. Ruano, and O. D. Sherby, Mater. Sci. Eng., A **317**, 101 (2001).

[54] C.-C. Fu, E. Meslin, A. Barbu, F. Willaime, and V. Oison, Solid State Phenom. **139**, 157 (2008).

[55] Although there exist several vacancy generation mechanisms in steady-state creep, the concentration of *mobile* vacancies at certain external conditions (applied stress and temperature) will decrease with increasing carbon content due to the strong driving force to form large and immobile Va$_1$C$_2$ complexes. These PDCs consequently lower self-diffusion and thus the vacancy binding rate to the dislocation core decreases. Therefore, the corresponding climb velocity (creep rate) is expected to decrease with increasing carbon content.

[56] J. P. Hirth and J. Lothe, *Theory of Dislocations* (Wiley, New York, 1982).

[57] N. F. Mott, Proc. Phys. Soc. London, Sect. B **64**, 729 (1951).